Eur. Phys. J. B (2017) 90: 239
DOI: 10.1140/epjb/e2017-80304-4

THE EUROPEAN PHYSICAL JOURNAL B

Regular Article

Entanglement spectra of superconductivity ground states on the honeycomb lattice

Sonja Predin[a] and John Schliemann

Institute for Theoretical Physics, University of Regensburg, D-93040 Regensburg, Germany

Received 29 May 2017 / Received in final form 20 September 2017
Published online 11 December 2017 –

Abstract. We analytically evaluate the entanglement spectra of the superconductivity states in graphene, primarily focusing on the s-wave and chiral $d_{x^2-y^2}+id_{xy}$ superconductivity states. We demonstrate that the topology of the entanglement Hamiltonian can differ from that of the subsystem Hamiltonian. In particular, the topological properties of the entanglement Hamiltonian of the chiral $d_{x^2-y^2}+id_{xy}$ superconductivity state obtained by tracing out one spin direction clearly differ from those of the time-reversal invariant Hamiltonian of noninteracting fermions on the honeycomb lattice.

1 Introduction

In graphene, the sixfold symmetry of the honeycomb lattice favors the degenerate $d_{x^2-y^2}$- and d_{xy}-wave superconductivity states. Recent theoretical studies have shown that a s-wave superconductivity state [1] and a chiral $d_{x^2-y^2}\pm id_{xy}$ superconducting state emerges from electron–electron interactions in graphene doped to the vicinity of the van-Hove singularity point [2–7], and in lower doped bilayer graphene [8–10] (for a recent review, see Ref. [11]). Below the superconducting transition temperature T_C, this degeneracy yields the time-reversal symmetry-breaking $d_{x^2-y^2}\pm id_{xy}$ state [11,12]. In the past two years, considerable experimental progress has been made regarding the observation of superconductivity in graphene. Evidence of superconductivity has been experimentally observed on Ca-intercalated bilayer graphene and graphene laminates at 4 [13] and 6.4 K [14], respectively. Furthermore, additional experimental progress has been made regarding evidence of superconductivity in Li-decorated monolayer graphene with a transition temperature of approximately 5.9 K [15].

The discovery of topological phases, which possess topological order and cannot be classified by a broken symmetry, has revealed the urgent need for a tool for characterization of these phases. It has been proven that the entanglement entropy obtained from the reduced density matrix can be an indicator of the topology in a system [16–18]. Further, Haldane and Li [19] have suggested that the entanglement spectrum of a system (the full set of eigenvalues of the reduced density matrix) contains more information about that system than the entanglement entropy, a single number. They have reported a remarkable relationship between the excitation spectrum and the edges separating the subsystems, considering the entanglement spectrum of the fractional quantum Hall system obtained using a spatial cut. It has been suggested that the entanglement spectrum constitutes a *tower of states*, which can be regarded as a fingerprint of the topological order [20–36] (for recent reviews, see Refs. [37,38]). The relationship between the entanglement, which can be calculated from the ground state, and the edge states, which are excited states of the Hamiltonian in a sample with boundaries, has been explored in this context. However, this relationship is not valid in general, as shown in references [39–41], in which the various entanglement spectra fail to describe the topological phase transitions.

The relationship between the entanglement spectrum obtained by tracing out one subsystem and the energy spectrum of the remaining subsystem is attracting considerable research attention. Particular focus has been placed on various spin ladder systems [42–50] and on bilayer systems [51–53], where a proportionality between the entanglement and subsystem Hamiltonians is realized by the strong coupling limit. However, this relationship is not valid in general, as indicated in reference [54], in which spin ladders of clearly nonidentical legs are studied, and in the case of graphene bilayers in the presence of trigonal warping [55].

In a two-dimensional topological superconductor with broken time-reversal symmetry, the topology can be characterized by a Chern number, which is an integral of the Berry curvature over the Brillouin zone. The entanglement Chern number C, i.e., the Chern number of the entanglement Hamiltonian obtained from the eigenvectors of that Hamiltonian, has been suggested to be a topological invariant of the entanglement Hamiltonian [55–57]. Note that some investigation of the relationship between the energetic and entanglement Hamiltonian topologies has already been performed [55].

[a] e-mail: sonja.predin@physik.uni-regensburg.de

In this paper, we present a fully analytical study of the entanglement spectrum of the fermionic ground state on a graphene honeycomb lattice, in the presence of superconductivity instability and as obtained by tracing out a single spin direction. We investigate the relationship between the entanglement and energy spectra of the remaining noninteracting part, placing a special focus on the correlation between their topologies. We show that the entanglement Hamiltonian obtained by tracing out one of the subsystems and the Hamiltonian of the remaining subsystem can have completely different topologies. This difference is due to the fact that the entanglement Hamiltonian is a ground-state property. That is, the $d_{x^2-y^2}+id_{xy}$ superconductivity state breaks the time-reversal symmetry of the superconductivity Hamiltonian; this behavior is reflected in the ground state of the composite superconductivity Hamiltonian. Further, the entanglement Hamiltonian is constructed from that ground state. We also discuss the case of sublattices B is traced out.

This paper is organized as follows: In Section 2, we introduce the model Hamiltonian and discuss the different superconductivity paired states that can arise on the honeycomb lattice. Classification of the topological phases of the superconductivity states on the honeycomb lattice based on their different symmetries is also performed in this section. The entanglement spectrum obtained from the Bardeen-Cooper-Schrieffer ground state by tracing out a single spin direction is analyzed in Section 3. Our primary interest in this section is to explore the relationship between the geometrical and topological properties of the entanglement Hamiltonian and the remaining noninteracting Hamiltonian. We close with a summary and an overview of the future research outlook, which is presented in Section 4. Some technical details on the analytical derivation of the full eigenstates of the noninteracting fermionic system on the honeycomb lattice in the presence of superconductivity instabilities are presented, along with correlation matrix calculations, in Appendices A and B.

2 Model Hamiltonian

The tight-binding Hamiltonian for free fermions on a graphene honeycomb lattice with a single $2p_z$ orbital per carbon (C) atom is

$$H_0 = -t\sum_{\langle ij\rangle}\sum_{\sigma=\uparrow,\downarrow}\left(a^\dagger_{i,\sigma}b_{j,\sigma}+h.c.\right) - \mu\sum_{i,\sigma}\left(a^\dagger_{i,\sigma}a_{i,\sigma}+b^\dagger_{i,\sigma}b_{i,\sigma}\right), \quad (1)$$

where t is the hopping energy between the nearest-neighbor C atoms, μ is the chemical potential and $a_{i,\sigma}$ ($a^\dagger_{i,\sigma}$) and $b_{i,\sigma}$ ($b^\dagger_{i,\sigma}$) are the onsite annihilation (creation) operators for electrons on sublattices A and B, respectively, with spin $\sigma=\uparrow,\downarrow$. Diagonalization of equation (1) yields the energy spectrum $\pm E_\pm$, with

$$E_\pm = \pm t|\gamma(\boldsymbol{k})| - \mu, \quad (2)$$

where $\gamma(\boldsymbol{k})=\sum_{\boldsymbol{\delta}}\exp(i\boldsymbol{k}\cdot\boldsymbol{\delta})$ and $\boldsymbol{\delta}$ is a nearest-neighbor vector. In what follows, we use coordinates with

$$\boldsymbol{\delta}_1 = a\left(0,\frac{1}{\sqrt{3}}\right), \quad (3)$$

$$\boldsymbol{\delta}_{2,3} = \frac{a}{2}\left(\pm1,-\frac{1}{\sqrt{3}}\right), \quad (4)$$

where $a=1.42\,\text{Å}$ is the distance between neighboring C atoms, such that the two inequivalent corners of the first Brillouin zone can be expressed as

$$\boldsymbol{K}_\pm = \pm\left(\frac{4\pi}{3a},0\right). \quad (5)$$

The energy spectrum of the free fermions over the first Brillouin zone is visualized in Figure 1.

In order to apply the mean-field approximation, we define the superconductivity order parameter as a three-component complex vector

$$\overrightarrow{\Delta} \equiv (\Delta_{\boldsymbol{\delta}_1},\Delta_{\boldsymbol{\delta}_2},\Delta_{\boldsymbol{\delta}_3}), \quad (6)$$

where the components are defined by

$$\Delta_{\boldsymbol{\delta}} = \langle a_{i\uparrow}b_{i+\boldsymbol{\delta}\downarrow} - a_{i\downarrow}b_{i+\boldsymbol{\delta}\uparrow}\rangle. \quad (7)$$

We study the superconductivity pairing arising from the nearest-neighbor attractive interaction

$$H_{int} = \sum_{i,\boldsymbol{\delta}}\Delta_{\boldsymbol{\delta}}\left(a^\dagger_{i\uparrow}b^\dagger_{i+\boldsymbol{\delta}\downarrow} - a^\dagger_{i\downarrow}b^\dagger_{i+\boldsymbol{\delta}\uparrow}\right), \quad (8)$$

with the limit of strong onsite interaction. The resulting mean-field Hamiltonian can be expressed in momentum space as

$$H_{MF} = -t\sum_{\boldsymbol{k}\sigma}\left(\gamma(\boldsymbol{k})a^\dagger_{\boldsymbol{k}\sigma}b_{\boldsymbol{k}\sigma}+h.c.\right) - \mu\sum_{\boldsymbol{k}\sigma}\left(a^\dagger_{\boldsymbol{k}\sigma}a_{\boldsymbol{k}\sigma}+b^\dagger_{\boldsymbol{k}\sigma}b_{\boldsymbol{k}\sigma}\right) - J\sum_{\boldsymbol{k},\boldsymbol{\delta}}\left(\Delta_{\boldsymbol{\delta}}e^{i\boldsymbol{k}\boldsymbol{\delta}}\left(a^\dagger_{\boldsymbol{k}\uparrow}b^\dagger_{-\boldsymbol{k}\downarrow}-a^\dagger_{\boldsymbol{k}\downarrow}b^\dagger_{-\boldsymbol{k}\uparrow}\right)+h.c.\right), \quad (9)$$

where J is the effective pairing potential arising from the electron–electron interaction. The kinetic part of the previous Hamiltonian can be diagonalized by introducing the following transformations

$$c_{\boldsymbol{k},\sigma} = \frac{1}{\sqrt{2}}(a_{\boldsymbol{k},\sigma}-e^{i\cdot\phi_{\boldsymbol{k}}}b_{\boldsymbol{k},\sigma}),$$
$$d_{\boldsymbol{k},\sigma} = \frac{1}{\sqrt{2}}(a_{\boldsymbol{k},\sigma}+e^{i\cdot\phi_{\boldsymbol{k}}}b_{\boldsymbol{k},\sigma}), \quad (10)$$

where the phase $\phi_{\boldsymbol{k}}$ is defined as $\phi_{\boldsymbol{k}}=\arg(\gamma_{\boldsymbol{k}})$. Note that $c^\dagger_{\boldsymbol{k},\boldsymbol{\sigma}}$ and $d^\dagger_{\boldsymbol{k},\boldsymbol{\sigma}}$ create an electron in the upper and lower Bogoliubov bands, respectively.

Thus, introducing the energy basis, the Hamiltonian becomes

$$H_{MF} = -t\sum_{\boldsymbol{k},\sigma}|\gamma_{\boldsymbol{k}}|(d^{\dagger}_{\boldsymbol{k},\sigma}d_{\boldsymbol{k},\sigma} - c^{\dagger}_{\boldsymbol{k},\sigma}c_{\boldsymbol{k},\sigma}) - \mu\sum_{\boldsymbol{k},\sigma}(d^{\dagger}_{\boldsymbol{k},\sigma}d_{\boldsymbol{k},\sigma} + c^{\dagger}_{\boldsymbol{k},\sigma}c_{\boldsymbol{k},\sigma}) - J\sum_{\boldsymbol{k}}\sum_{\boldsymbol{\delta}}\Big(\Delta_{\boldsymbol{\delta}}\Big(\cos(\boldsymbol{k\delta}-\phi_{\boldsymbol{k}})(d^{\dagger}_{\boldsymbol{k},\uparrow}d^{\dagger}_{-\boldsymbol{k},\downarrow} - c^{\dagger}_{\boldsymbol{k},\uparrow}c^{\dagger}_{-\boldsymbol{k},\downarrow}) + i\sin(\boldsymbol{k\delta}-\phi_{\boldsymbol{k}})(c^{\dagger}_{\boldsymbol{k},\uparrow}d^{\dagger}_{-\boldsymbol{k},\downarrow} - d^{\dagger}_{\boldsymbol{k},\uparrow}c^{\dagger}_{-\boldsymbol{k},\downarrow})\Big) + h.c.\Big). \quad (11)$$

The third line in this Hamiltonian is the intraband pairing, containing an order parameter that is even in k-space and corresponding to the spin-singlet pairing. The fourth line is the interband pairing, containing an order parameter that is odd in k-space and corresponding to the spin-triplet pairing. We use the definitions

$$C_{\boldsymbol{k}} = J\sum_{\boldsymbol{\delta}}\Delta_{\boldsymbol{\delta}}\cos(\boldsymbol{k\delta}-\phi_{\boldsymbol{k}}), \quad (12)$$

and

$$S_{\boldsymbol{k}} = J\sum_{\boldsymbol{\delta}}\Delta_{\boldsymbol{\delta}}\sin(\boldsymbol{k\delta}-\phi_{\boldsymbol{k}}). \quad (13)$$

The corresponding span of the superconducting order parameter is

$$\overrightarrow{\Delta} = \begin{cases} \Delta(1,1,1), \\ \Delta(2,-1,-1), \\ \Delta(0,-1,1), \end{cases} \quad (14)$$

where Δ is the self-consistent superconductivity order parameter. In what follows, we use the redefinition $J\Delta \equiv \Delta$. The linearized self-consistence equations of the order parameter are invariant with respect to the hexagonal group C_{6v} [2], i.e., the symmetry group of the honeycomb lattice. The first solution corresponds to the s-wave, $\overrightarrow{\Delta} = \Delta(1,1,1)$, belonging to the natural A1 irreducible representation of the C_{6v} group of the honeycomb lattice. The A1 irreducible representation is spanned by the vector $\boldsymbol{u}_1 = (1,1,1)$. The final two solutions, $\overrightarrow{\Delta} = \Delta(2,-1,-1)$ and $\overrightarrow{\Delta} = \Delta(0,-1,1)$, belong to the two-dimensional subspace of the S_3 group [58], the span of which is $\boldsymbol{u}_2 = (2,-1,-1)$ and $\boldsymbol{u}_3 = (0,-1,1)$. The second (corresponding to the $d_{x^2-y^2}$ wave) and third (corresponding to the d_{xy} wave) solutions belong to the E1 and E2 irreducible representations of the S_3 group, respectively. From the symmetry perspective, it is noteworthy that every combination of the $d_{x^2-y^2}$ and d_{xy} waves is possible. However, it has been shown that the $d_{x^2-y^2} \pm id_{xy}$-wave superconductivity state with an order parameter

$$\overrightarrow{\Delta}_{d_{x^2-y^2}\pm id_{xy}} = \frac{1}{\sqrt{3}}\Delta\begin{pmatrix} 1 \\ e^{\pm\frac{2i\pi}{3}} \\ e^{\mp\frac{2i\pi}{3}} \end{pmatrix}, \quad (15)$$

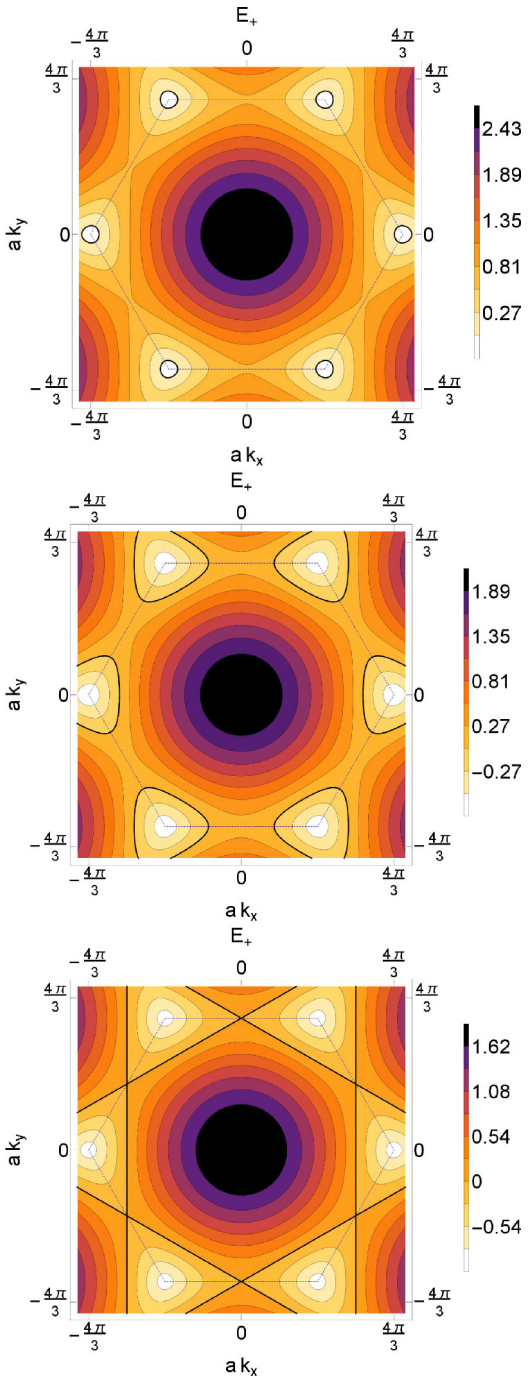

Fig. 1. Brillouin zone with density plot of $|\gamma(\boldsymbol{k})| - \frac{\mu}{t}$ for: (a) $\frac{\mu}{t} = 0.2$; (b) $\frac{\mu}{t} = 0.8$; and (c) $\frac{\mu}{t} = 1$. The edge of the first Brillouin zone is marked by dashed blue lines.

is preferred in graphene below T_C for a superconductivity coupling strength J that is not excessively large, and for doping up to and in the vicinity of the van-Hove singularity point [2].

The s-wave superconductivity order parameter is given by $\Delta(\boldsymbol{k}) = \gamma(\boldsymbol{k})$, while the $d_{x^2-y^2} + id_{xy}$-wave superconductivity order parameter is

$$\Delta_{d\pm id}(\boldsymbol{k}) = \cos\left(\frac{\pi}{3}\right)\Delta_{d_{x^2-y^2}}(\boldsymbol{k}) \pm \sin\left(\frac{\pi}{3}\right)\Delta_{d_{xy}}(\boldsymbol{k}), \quad (16)$$

with

$$\Delta_{d_{x^2-y^2}}(\boldsymbol{k}) = 2\Delta\left(e^{iak_x} - e^{-i\frac{a}{2}k_x}\cos(\frac{a\sqrt{3}}{2}k_y)\right), \quad (17)$$

$$\Delta_{d_{xy}}(\boldsymbol{k}) = -2i\Delta\sin\left(\frac{a\sqrt{3}}{2}k_y\right)e^{-i\frac{a}{2}k_x}. \quad (18)$$

Introducing the spinor

$$\varphi^\dagger_{\boldsymbol{k}} = \left(a^\dagger_{\boldsymbol{k}\uparrow}, b^\dagger_{\boldsymbol{k}\uparrow}, a^\dagger_{\boldsymbol{k}\downarrow}, b^\dagger_{\boldsymbol{k}\downarrow}, a_{-\boldsymbol{k}\uparrow}, b_{-\boldsymbol{k}\uparrow}, a_{-\boldsymbol{k}\downarrow}, b_{-\boldsymbol{k}\downarrow}\right), \quad (19)$$

the Hamiltonian of equation (9) can be expressed as

$$H_{MF} = \frac{1}{2}\sum_{\boldsymbol{k}}\varphi^\dagger_{\boldsymbol{k}}\mathcal{M}_{\boldsymbol{k}}\varphi_{\boldsymbol{k}}, \quad (20)$$

where

$$\mathcal{M}_{\boldsymbol{k}} = \begin{pmatrix} \zeta(\boldsymbol{k}) & 0 & 0 & -\overline{\Delta}(\boldsymbol{k}) \\ 0 & \zeta(\boldsymbol{k}) & \overline{\Delta}(\boldsymbol{k}) & 0 \\ 0 & \overline{\Delta}^*(-\boldsymbol{k}) & -\zeta^*(-\boldsymbol{k}) & 0 \\ -\overline{\Delta}^*(-\boldsymbol{k}) & 0 & 0 & -\zeta^*(-\boldsymbol{k}) \end{pmatrix}, \quad (21)$$

with

$$\zeta(\boldsymbol{k}) = \begin{pmatrix} -\mu & -t\gamma(\boldsymbol{k}) \\ -t\gamma^*(\boldsymbol{k}) & -\mu \end{pmatrix}, \quad (22)$$

$$\overline{\Delta}(\boldsymbol{k}) = \begin{pmatrix} 0 & \Delta(\boldsymbol{k}) \\ \Delta(-\boldsymbol{k}) & 0 \end{pmatrix}. \quad (23)$$

The resultant Hamiltonian indicates that the spin-singlet superconductivity state without spin-orbit coupling is invariant under the spin SU(2) rotation. Hence, we obtain the condition

$$[J_i, \mathcal{M}(\boldsymbol{k})] = 0, \quad J_i = \begin{pmatrix} s_i & 0 \\ 0 & -s_i^* \end{pmatrix}, \ (i = x, y, z). \quad (24)$$

As a result of the spin SU(2) rotation, it is sufficient to use the spinor $\Psi^\dagger_{\boldsymbol{k}} = (a^\dagger_{\boldsymbol{k}\uparrow}, b^\dagger_{\boldsymbol{k}\uparrow}, a_{-\boldsymbol{k}\downarrow}, b_{-\boldsymbol{k}\downarrow})$ in order to express the Hamiltonian of the superconductivity state on the honeycomb lattice in the form

$$H_{MF} = \sum_{\boldsymbol{k}}\Psi^\dagger_{\boldsymbol{k}}h(\boldsymbol{k})\Psi_{\boldsymbol{k}}, \quad (25)$$

where

$$h(\boldsymbol{k}) = \begin{pmatrix} -\mu & -t\gamma(\boldsymbol{k}) & 0 & -\Delta(\boldsymbol{k}) \\ -t\gamma^*(\boldsymbol{k}) & -\mu & -\Delta(-\boldsymbol{k}) & 0 \\ 0 & -\Delta^*(-\boldsymbol{k}) & \mu & t\gamma^*(-\boldsymbol{k}) \\ -\Delta^*(\boldsymbol{k}) & 0 & t\gamma(-\boldsymbol{k}) & \mu \end{pmatrix}. \quad (26)$$

When the superconductivity order parameter is pure real the Hamiltonian $h(\boldsymbol{k})$ satisfies

$$Th(\boldsymbol{k})T^{-1} = h(-\boldsymbol{k}), \quad (27)$$

where $T = K$ mimics time-reversal symmetry. The condition given in equation (27) can satisfy a real superconductivity order parameter only. The $d_{x^2-y^2} + id_{xy}$-wave superconductivity order parameter given by equation (16) breaks the time-reversal symmetry. It appertains to the CI-class in the Altland-Zirnbauer classification of topological insulators and superconductors [59–61]. Furthermore, it is possible to classify two-dimensional C-class superconductors using the Chern number C. Note that the nontrivial topology of the $d_{x^2-y^2} + id_{xy}$-wave superconductivity state is denoted by the Chern number $C = 2$.

3 Entanglement spectra

A method for analytically calculating the entanglement spectrum of a free-fermion system is given in references [52,62,63]. Here, we generalize this method to superconductivity systems, using an approach similar to that described in references [64,65].

The entanglement Hamiltonian can be constructed as a single-particle operator in a quadratic matrix [52,62,63], as it is completely determined by any correlation matrix of operators acting on the remaining part after the subsystem has been traced out. Our system consists of two subsystems, A and B. The reduced density matrix for subsystem A, defined as $\rho_A = \mathrm{tr}_B\rho$, can be formulated as in the free fermion case, such that $\rho_A = \frac{1}{Z}e^{-H_{\mathrm{ent}}}$, using the entanglement spectrum H_{ent} and the partition function $Z = \mathrm{tr}\left(e^{-H_{\mathrm{ent}}}\right)$. Furthermore, the average $\langle\mathcal{O}\rangle$ of a local operator in subsystem A can be calculated as $\langle\mathcal{O}\rangle = \mathrm{tr}(\rho_A\mathcal{O}_A)$.

By tracing out a single spin direction, e.g., the negative spin $\downarrow$, from the ground state on the honeycomb lattice in the presence of the s-wave and chiral $d + id$-wave superconductivity, the correlation matrix can be formulated as

$$C(\boldsymbol{k}) = \begin{pmatrix} \langle a^\dagger_{\boldsymbol{k}\uparrow}a_{\boldsymbol{k}\uparrow}\rangle & \langle a^\dagger_{\boldsymbol{k}\uparrow}b_{\boldsymbol{k}\uparrow}\rangle \\ \langle b^\dagger_{\boldsymbol{k}\uparrow}a_{\boldsymbol{k}\uparrow}\rangle & \langle b^\dagger_{\boldsymbol{k}\uparrow}b_{\boldsymbol{k}\uparrow}\rangle \end{pmatrix}. \quad (28)$$

For more technical details of the analytical calculations of the correlation matrix, we refer the reader to Appendix B. Here, one can show that the eigenvalues of the correlation matrix η_l are related to the entanglement spectrum ξ_l, such that

$$\xi_l = \ln\left(\frac{1-\eta_l}{\eta_l}\right). \quad (29)$$

3.1 s-wave scenario

The s-wave superconductivity order parameter corresponds to the bond-independent superconductivity state; thus, $S_{\boldsymbol{k}}$ is identically zero.

We analytically obtain the entanglement levels (Eq. (29))

$$\xi_1(\boldsymbol{k}) = -2\mathrm{arcsinh}\left(\frac{t|\gamma(\boldsymbol{k})| + \mu}{|C_{\boldsymbol{k}}|}\right) \quad (30)$$

and

$$\xi_2(\boldsymbol{k}) = 2\text{arcsinh}\left(\frac{t|\gamma(\boldsymbol{k})| - \mu}{|C_{\boldsymbol{k}}|}\right). \tag{31}$$

The entanglement Hamiltonian has the form

$$\mathcal{H}_{ent} = \sum_{\boldsymbol{k}} \left(\xi_1 e^{\dagger}_{\boldsymbol{k},+} e_{\boldsymbol{k},+} + \xi_2 f^{\dagger}_{\boldsymbol{k},+} f_{\boldsymbol{k},+}\right), \tag{32}$$

where $e_{\boldsymbol{k},+}$ and $f_{\boldsymbol{k},+}$ are Bogoliubov transformations given in Appendix B by equations (B.1) and (B.2). The entanglement levels for different values of μ, with $t = 2.5\,\text{eV}$, and $\Delta = 3\,\text{eV}$ are shown in Figure 2.

The undoped graphene is a gapless semi-metal and is not a superconductor at low temperatures. However, when the system is at half-filling (with $\mu = 0$), the entanglement levels are

$$\xi_{1,2}(\boldsymbol{k}) = \pm 2\text{arcsinh}\left(\frac{t}{\Delta}\right), \tag{33}$$

being constant over the entire Brillouin zone. In the strong coupling regime, when $\Delta \gg t$, one finds

$$\xi_{1,2}(\boldsymbol{k}) \approx \pm 2\frac{t}{\Delta}. \tag{34}$$

The canonical entanglement Hamiltonian at half-filling is independent of the inverse temperature [53] $\beta = k_E/\Delta$, such that

$$\mathcal{H}_{can} = \sum_{i=1}^{2} \frac{1}{k_E}\left(e^{\dagger}_{\boldsymbol{k},+} e_{\boldsymbol{k},+} + f^{\dagger}_{\boldsymbol{k},+} f_{\boldsymbol{k},+}\right), \tag{35}$$

where k_E is a constant. In general, there is no proportionality between the entanglement Hamiltonian and the energy Hamiltonian of free fermions, because the coupling between subsystems $C_{\boldsymbol{k}}$ is $\boldsymbol{k}$-dependent in the Brillouin zone. When $C_{\boldsymbol{k}} = 0$, at the Dirac points, the entanglement levels are not entangled. However, at finite doping, the maximally entangled states, when the entanglement levels are zero, correspond to the zero-energy state of the noninteracting fermions. To provide a superior visualization, a thick black line is used to connect the zero-energy states in Figure 1 and the maximally entangled states in Figure 2.

3.2 Chiral d-wave scenario

To enable analytical calculations, we diagonalize the Hamiltonian (26)

$$H_{MF} = \sum_{\boldsymbol{k}} E_\alpha (o^{\dagger}_{\boldsymbol{k},+} o_{\boldsymbol{k},+} + o^{\dagger}_{-\boldsymbol{k},-} o_{-\boldsymbol{k},-}) + \sum_{\boldsymbol{k}} E_\beta (p^{\dagger}_{\boldsymbol{k},+} p_{\boldsymbol{k},+} + p^{\dagger}_{-\boldsymbol{k},-} p_{-\boldsymbol{k},-}), \tag{36}$$

by the Bogoliubov quasiparticles $o_{\boldsymbol{k},+}, o_{-\boldsymbol{k},-}, p_{\boldsymbol{k},+}$ and $p_{-\boldsymbol{k},-}$ given in Appendix A with equations (A.30) and (A.31). The energies of the Bogoliubov quasiparticles are $\pm E_\alpha$ and $\pm E_\beta$, where

$$E_\alpha = \sqrt{t^2|\gamma(\boldsymbol{k})|^2 + \mu^2 + (|S_{\boldsymbol{k}}|^2 + |C_{\boldsymbol{k}}|^2) + 2\sqrt{u+v}}, \tag{37}$$

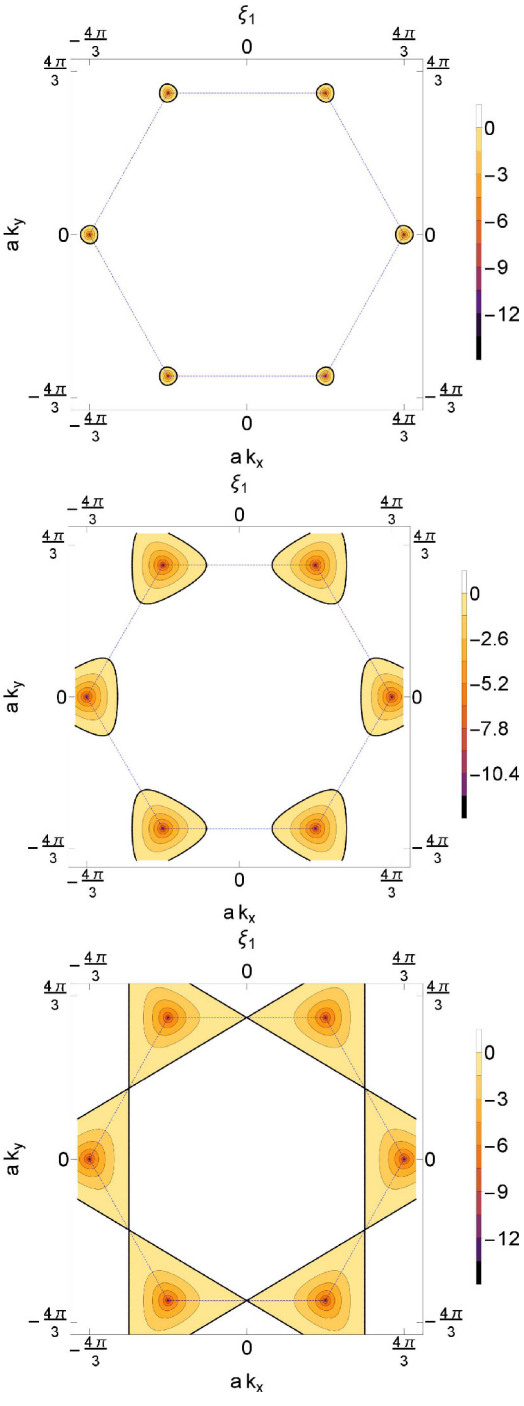

Fig. 2. Contour plot of entanglement level $\xi_1(\boldsymbol{k})$ of s-wave superconductivity state on honeycomb lattice plotted for $\frac{J}{t} = 3$ and: (a) $\frac{\mu}{t} = 0.2$; (b) $\frac{\mu}{t} = 0.8$; and (c) $\frac{\mu}{t} = 1$. The thin blue dashed and thick black lines represent the first Brillouin zone and connect the zero energy states, respectively.

and

$$E_\beta = \sqrt{t^2|\gamma(\boldsymbol{k})|^2 + \mu^2 + (|S_{\boldsymbol{k}}|^2 + |C_{\boldsymbol{k}}|^2) - 2\sqrt{u+v}} \quad (38)$$

with

$$u = \left(\mu^2 + |S_{\boldsymbol{k}}|^2\right) t^2|\gamma(\boldsymbol{k})|^2, \quad (39)$$

and

$$v = \left(\mathrm{Re}(C_{\boldsymbol{k}})\mathrm{Im}(S_{\boldsymbol{k}}) - \mathrm{Re}(S_{\boldsymbol{k}})\mathrm{Im}(C_{\boldsymbol{k}})\right)^2. \quad (40)$$

When the superconductivity order parameters $\Delta_{\boldsymbol{\delta}}$ are pure real, i.e., when no time-reversal symmetry breaking occurs, v vanishes.

From analytical calculations, one obtains the correlation matrix at $T = 0$

$$C(\boldsymbol{k}) = \begin{pmatrix} C_{11}(\boldsymbol{k}) & C_{12}(\boldsymbol{k}) \\ C_{12}^*(\boldsymbol{k}) & C_{22}(\boldsymbol{k}) \end{pmatrix}, \quad (41)$$

where

$$\begin{aligned} C_{11} &= \langle a_{\boldsymbol{k}\uparrow}^\dagger a_{\boldsymbol{k}\uparrow}\rangle \\ &= \frac{1}{2} + \frac{1}{4}\frac{\mu}{\sqrt{\mu^2 + |S_{\boldsymbol{k}}|^2}}(\epsilon_1 + m) \\ &\quad \times \frac{1}{E_\alpha}\left(1 - \frac{m}{\sqrt{t^2|\gamma(\boldsymbol{k})|^2 + m^2}}\right) \\ &\quad + \frac{1}{4}\frac{\mu}{\sqrt{\mu^2 + |S_{\boldsymbol{k}}|^2}}(\epsilon_2 + m) \\ &\quad \times \frac{1}{E_\beta}\left(1 + \frac{m}{\sqrt{t^2|\gamma(\boldsymbol{k})|^2 + m^2}}\right), \end{aligned} \quad (42)$$

$$\begin{aligned} C_{22} &= \langle b_{\boldsymbol{k}\uparrow}^\dagger b_{\boldsymbol{k}\uparrow}\rangle \\ &= \frac{1}{2} + \frac{1}{4}\frac{\mu}{\sqrt{\mu^2 + |S_{\boldsymbol{k}}|^2}}(\epsilon_1 - m) \\ &\quad \times \frac{1}{E_\alpha}\left(1 + \frac{m}{\sqrt{t^2|\gamma(\boldsymbol{k})|^2 + m^2}}\right) \\ &\quad + \frac{1}{4}\frac{\mu}{\sqrt{\mu^2 + |S_{\boldsymbol{k}}|^2}}(\epsilon_2 - m) \\ &\quad \times \frac{1}{E_\beta}\left(1 - \frac{m}{\sqrt{t^2|\gamma(\boldsymbol{k})|^2 + m^2}}\right), \end{aligned} \quad (43)$$

$$\begin{aligned} C_{12} &= \langle a_{\boldsymbol{k}\uparrow}^\dagger b_{\boldsymbol{k}\uparrow}\rangle \\ &= \frac{1}{4}e^{-i\phi_{\boldsymbol{k}}}\left(\left(\frac{\epsilon_1}{E_\alpha} - \frac{\epsilon_2}{E_\beta}\right) - in\left(\frac{1}{E_\alpha} - \frac{1}{E_\beta}\right)\right) \\ &\quad \times \frac{t|\gamma(\boldsymbol{k})|}{\sqrt{t^2|\gamma(\boldsymbol{k})|^2 + m^2}} \end{aligned} \quad (44)$$

with

$$\epsilon_{1,2} = \sqrt{\mu^2 + |S_{\boldsymbol{k}}|^2} \pm \sqrt{t^2|\gamma(\boldsymbol{k})|^2 + m^2}, \quad (45)$$

while

$$m = \frac{\mathrm{Re}(\mathrm{C}_{\boldsymbol{k}}) \cdot \mathrm{Im}(\mathrm{S}_{\boldsymbol{k}}) - \mathrm{Im}(\mathrm{C}_{\boldsymbol{k}}) \cdot \mathrm{Re}(\mathrm{S}_{\boldsymbol{k}})}{\sqrt{\mu^2 + |S_{\boldsymbol{k}}|^2}}, \quad (46)$$

and

$$n = \frac{\mathrm{Re}(C_{\boldsymbol{k}})\mathrm{Re}(S_{\boldsymbol{k}}) + \mathrm{Im}(C_{\boldsymbol{k}})\mathrm{Im}(S_{\boldsymbol{k}})}{\sqrt{\mu^2 + |S_{\boldsymbol{k}}|^2}}. \quad (47)$$

Thus, the entanglement spectrum obtained from the eigenvalues of the correlation matrix given in equation (29) consists of entanglement levels ξ_1 and ξ_2 where:

$$\begin{aligned} \xi_{1,2} = &-2\mathrm{arctanh} \\ &\times(C_{11} + C_{22} - 1 \pm \sqrt{(C_{11} - C_{22})^2 + 4|C_{12}|^2}). \end{aligned} \quad (48)$$

As the d-wave spin-singlet superconductivity order parameter involves both $C_{\boldsymbol{k}}$ and $S_{\boldsymbol{k}}$, there is no relationship between states with the zero-value states of the entanglement spectrum and the zero-energy states of the free fermions. At the van-Hove singularity point, i.e., when $\mu = t$, both the entanglement spectrum and the energy spectrum of the free fermions are zero at the M point. The results of our analytical calculations of the entanglement spectrum of the $d_{x^2-y^2} + id_{xy}$-wave superconductivity on the honeycomb lattice are presented in Figure 3.

As we have discussed above, the $d_{x^2-y^2}$- and d_{xy}-wave superconductivity order parameters preserve the time-reversal symmetry (Eq. (27)). Based on the time-reversal symmetry and provided $\Psi_{\boldsymbol{k}}$ are the eigenstates of the Hamiltonian given in equation (26), we can state that

$$\Psi_{\boldsymbol{k}}^* = \Psi_{-\boldsymbol{k}}, \quad (49)$$

where the $\Psi_{-\boldsymbol{k}}^*$ are also eigenstates of the Hamiltonian of equation (26). This yields

$$\Phi_{\boldsymbol{k}}^* = \Phi_{-\boldsymbol{k}}. \quad (50)$$

Hence, the real d-wave superconductivity order parameter preserves the time-reversal symmetry in the correlation matrix, which is constructed from the $\Phi_{\boldsymbol{k}}$ as $C(\boldsymbol{k}) = \langle\Phi_{\boldsymbol{k}}^\dagger\Phi_{\boldsymbol{k}}\rangle$. The entanglement Hamiltonian satisfies:

$$T_E\mathcal{H}_{ent}(\boldsymbol{k})T_E^{-1} = \mathcal{H}_{ent}(-\boldsymbol{k}), \quad (51)$$

with $T_E = K$.

When the $d_{x^2-y^2} + id_{xy}$-wave superconductivity order parameter is considered, $C_{\boldsymbol{k}}$ and $S_{\boldsymbol{k}}$ are complex functions. Then, the m and n terms are non-zero. Hence, the average occupancy number at site A, $C_{11}(\boldsymbol{k})$, and the average occupancy number at site B, $C_{22}(\boldsymbol{k})$, are not equal and the off-diagonal element of the correlation matrix $C_{12}(\boldsymbol{k})$ is complex. Because $S_{\boldsymbol{k}}$ is an odd

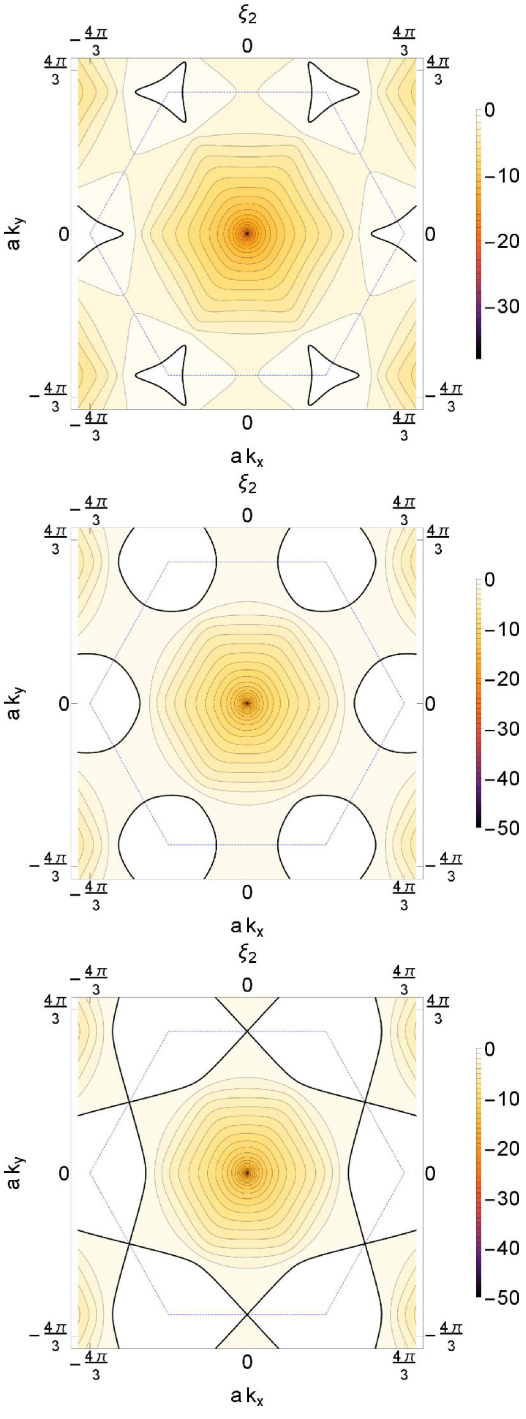

Fig. 3. Contour plot of the entanglement level $\xi_1(\boldsymbol{k})$ of $d_{x^2-y^2}+id_{xy}$-wave superconductivity state on the honeycomb lattice plotted for $\frac{J}{t}=3$ and (a) $\frac{\mu}{t}=0.2$, (b) $\frac{\mu}{t}=0.8$ and (c) $\frac{\mu}{t}=1$. The dashed blue line delineates the first Brillouin zone, while the thick black line shows maximally entangled states.

function in the momentum space, while $C_{\boldsymbol{k}}$ is a even function, it can be shown that elements of the correlation matrix $C_{11}(\boldsymbol{k})$, $C_{22}(\boldsymbol{k})$, and $C_{12}(\boldsymbol{k})$ are constrained as $C_{11}(-\boldsymbol{k})=C_{22}(\boldsymbol{k})$ and $C^*_{12}(-\boldsymbol{k})=C_{12}(\boldsymbol{k})$. Therefore, it follows that the complex $d_{x^2-y^2}+id_{xy}$-wave superconductivity order parameter breaks the time-reversal symmetry in the entanglement Hamiltonian. The topology of the entanglement Hamiltonian in two-dimension with broken time-reversal symmetry is characterized by the entanglement Chern number.

For further analysis of the topological properties of the entanglement Hamiltonian, we require not only its eigenvalues, but also its eigenstates. The eigenstates of the correlation matrix are identical to the eigenstates of the entanglement Hamiltonian and can be expressed as

$$q_{\boldsymbol{k}\uparrow}=\delta_+(\boldsymbol{k})a_{\boldsymbol{k}\uparrow}+\delta_-(\boldsymbol{k})b_{\boldsymbol{k}\uparrow}, \tag{52}$$
$$r_{\boldsymbol{k}\uparrow}=\delta_+(-\boldsymbol{k})a_{\boldsymbol{k}\uparrow}-\delta^*_-(-\boldsymbol{k})b_{\boldsymbol{k}\uparrow}, \tag{53}$$

where explicit expressions for $\delta_+(\boldsymbol{k})$ and $\delta_-(\boldsymbol{k})$ are given in Appendix B by equation (B.17). Using these eigenstates, we can calculate the Berry curvature

$$F(\boldsymbol{k})=\frac{\partial A_y}{\partial k_x}-\frac{\partial A_x}{\partial k_y} \tag{54}$$

and the Berry connection

$$\boldsymbol{A}(\boldsymbol{k})=i\langle r(\boldsymbol{k})|\frac{\partial}{\partial \boldsymbol{k}}|r(\boldsymbol{k})\rangle, \tag{55}$$

which vanish everywhere outside the Dirac points where quantized "monopole" sources of the δ-function type exist.

Through numerical integrations of the Berry curvature along the Brillouin zone, we find that the entanglement Chern number is $C=1$, in the case of the chiral $d_{x^2-y^2}+id_{xy}$-wave superconductivity state. In the presence of $SU(2)$ rotation and broken time-reversal symmetry, as in the case of an energetic Hamiltonian, the Chern number C can have even values only. For the entanglement Hamiltonian, it is possible to obtain an odd value for the Chern number, as it is not invariant to the $SU(2)$ rotation. As a result, the topology of the entanglement Hamiltonian, which is obtained by tracing out the spin-down subsystem of the ground state of the chiral $d_{x^2-y^2}+id_{xy}$-wave superconductivity state on the honeycomb lattice, clearly differs from the topology of the energetic Hamiltonian of free fermions without the superconductivity instabilities.

3.3 Tracing out B sublattices

3.3.1 s-wave scenario

We will now consider the ground state of interacting fermions on the honeycomb lattice in the presence of the s-wave superconductivity instability. Upon tracing out B sublattices the entanglement levels:

$$\xi_\pm=\pm 2\text{arctanh}\left(\frac{t^2|\gamma(\boldsymbol{k})|^2-\mu^2+\Delta^2|\gamma(\boldsymbol{k})|^2}{E_\alpha E_\beta}\right), \tag{56}$$

where $E_\alpha=\sqrt{(t|\gamma(\boldsymbol{k})|-\mu)^2+\Delta^2|\gamma(\boldsymbol{k})|^2}$ and $E_\beta=\sqrt{(t|\gamma(\boldsymbol{k})|+\mu)^2+\Delta^2|\gamma(\boldsymbol{k})|^2}$. When system is at half-filling the subsystems are maximally entangled. The entanglement levels are plotted at Figure 4.

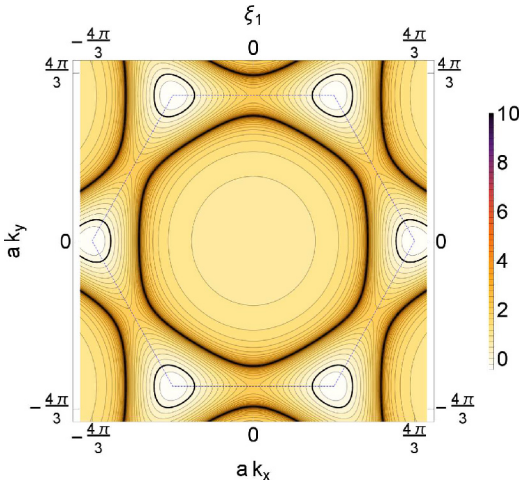

Fig. 4. Contour plot of entanglement level $\xi_1(\boldsymbol{k})$ of s-wave superconductivity state on honeycomb lattice plotted for $\frac{J}{t}=3$ and $\frac{\mu}{t}=0.8$. The first Brillouin zone is border by the dashed blue line, while the thick line connects maximally entangled states.

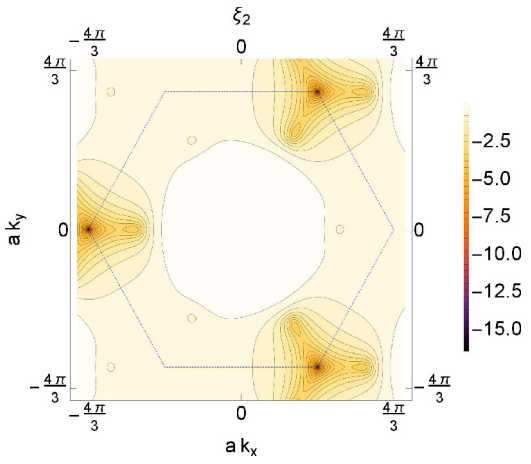

Fig. 5. Contour plot of entanglement level $\xi_2(\boldsymbol{k})$ of $d_{x^2-y^2}+id_{xy}$ superconductivity state on honeycomb lattice plotted for $\frac{J}{t}=3$ and $\frac{\mu}{t}=0.8$. The thin blue dashed and thick black lines represent the first Brillouin zone and connect the zero energy states, respectively.

3.3.2 Chiral d-wave scenario

Upon tracing out B sublattices, the entanglement spectrum of d-wave superconductivity state on the honeycomb lattice is completely determined by the correlation matrix:

$$C(\boldsymbol{k})=\begin{pmatrix} C_{11}(\boldsymbol{k}) & C_{13}(\boldsymbol{k}) \\ C_{13}^{*}(\boldsymbol{k}) & C_{33}(\boldsymbol{k}) \end{pmatrix}, \tag{57}$$

where C_{11}, C_{33} and C_{13} are given in Appendix B. The eigenvalues $\eta_{1,2}$ of the correlation matrix

$$\eta_{1,2}=\frac{1}{2}\left((C_{11}+C_{33}+\pm\sqrt{(C_{11}-C_{33})^2+4|C_{13}|^2}\right). \tag{58}$$

are related to the entanglement levels $\xi_{1,2}=\ln\left(\frac{\eta_{\pm}}{1-\eta_{pm}}\right)$. At finite doping the entanglement levels never vanish. Here, space inversion symmetry of the entanglement spectrum is broken and the entanglement levels satisfy $\xi_{\pm}(-\boldsymbol{k})=-\xi_{\mp}(\boldsymbol{k})$. The entanglement level $\xi_2(\boldsymbol{k})$ is visualized in Figure 5. The broken time-reversal symmetry in the entanglement Hamiltonian leads to the entanglement Chern number $C=1$.

4 Conclusion and outlook

We analytically evaluated the entanglement spectra of the superconductivity states on the graphene honeycomb lattice, primarily focusing on the s-wave and chiral $d_{x^2-y^2}+id_{xy}$ superconductivity states. When one spin direction was traced out, exact correspondence between the maximally entangled states of the s-wave superconductor and the zero energies of the noninteracting fermionic honeycomb lattice at finite doping was observed. The relationship between the topologies of the entanglement and subsystem Hamiltonians was found to depend on the coupling between the subsystems. Further, the chiral $d_{x^2-y^2}+id_{xy}$ superconductivity order parameter breaks the time-reversal symmetry in the entanglement Hamiltonian. The topological properties of the entanglement Hamiltonian, characterized by the topological nontrivial entanglement Chern number $C=1$, clearly differ from those of the time-reversal invariant Hamiltonian of the noninteracting fermions on the honeycomb lattice. The investigations presented herein are based on closed analytical expressions for the full eigensystems of the s- and d-wave superconductivity states on the honeycomb lattice over the entire Brillouin zone. The method used to examine these eigensystems may constitute a useful tool for new studies of superconductivity in graphene. Future work may investigate the relationship between the topologies of the entanglement and subsystem Hamiltonians through the topological phase transition; for example, in the coexistence region between antiferromagnetism and $d_{x^2-y^2}+id_{xy}$ superconducting correlations in graphene [66] and graphene bilayers [8].

The authors kindly acknowledge Milica V. Milovanović. This work was supported by Deutsche Forschungsgemeinschaft via GRK1570.

Appendix A: Derivation of the eigensystem

In this appendix we present analytical diagonalization of the Hamiltonian of the chiral $d+id$-wave superconductivity state on the honeycomb lattice. Complexity of the order parameter makes the analytical approach more difficult. The starting point of our analysis is the Bardeen-Cooper-Schrieffer mean-field Hamiltonian in

$$H_1(\boldsymbol{k}) = \begin{pmatrix} t|\gamma(\boldsymbol{k})| - \mu & 0 & C_{\boldsymbol{k}} & -iS_{\boldsymbol{k}} \\ 0 & -t|\gamma(\boldsymbol{k})| - \mu & iS_{\boldsymbol{k}} & -C_{\boldsymbol{k}} \\ C^*_{\boldsymbol{k}} & -iS^*_{\boldsymbol{k}} & -t|\gamma(\boldsymbol{k})| + \mu & 0 \\ iS^*_{\boldsymbol{k}} & -C^*_{\boldsymbol{k}} & 0 & t|\gamma(\boldsymbol{k})| + \mu \end{pmatrix} \tag{A.4}$$

$$H_1^{'}(\boldsymbol{k}) = \begin{pmatrix} t|\gamma(\boldsymbol{k})| - \mu & 0 & 0 & -iS_{\boldsymbol{k}} \\ 0 & -t|\gamma(\boldsymbol{k})| - \mu & iS_{\boldsymbol{k}} & 0 \\ 0 & -iS^*_{\boldsymbol{k}} & -t|\gamma(\boldsymbol{k})| + \mu & 0 \\ iS^*_{\boldsymbol{k}} & 0 & 0 & t|\gamma(\boldsymbol{k})| + \mu \end{pmatrix} \tag{A.5}$$

momentum space

$$\begin{aligned} H_{MF}(\boldsymbol{k}) &= -t\sum_{\boldsymbol{k}} \left(\gamma(\boldsymbol{k}) a^\dagger_{\boldsymbol{k}\sigma} b_{\boldsymbol{k}\sigma} + h.c.\right) \\ &- \mu \sum_{\boldsymbol{k}} \left(a^\dagger_{\boldsymbol{k}\sigma} a_{\boldsymbol{k}\sigma} + b^\dagger_{\boldsymbol{k}\sigma} b_{\boldsymbol{k}\sigma}\right) \\ &- J\sum_{\boldsymbol{k},\boldsymbol{\delta}} \left(\Delta_{\boldsymbol{\delta}} e^{i\boldsymbol{k}\boldsymbol{\delta}} \left(a^\dagger_{\boldsymbol{k}\uparrow} b^\dagger_{-\boldsymbol{k}\downarrow} - a^\dagger_{\boldsymbol{k}\downarrow} b^\dagger_{-\boldsymbol{k}\uparrow}\right) + h.c.\right), \end{aligned} \tag{A.1}$$

where we define the superconductivity order parameter

$$\Delta(\boldsymbol{k}) = \sum_{\boldsymbol{\delta}} \Delta_{\boldsymbol{\delta}} e^{i\boldsymbol{k}\boldsymbol{\delta}}, \tag{A.2}$$

as a combination of the $d_{x^2-y^2}$ and d_{xy}-wave superconductivity state $\Delta_{d\pm id}(\boldsymbol{k}) = \cos\left(\frac{\pi}{3}\right)\Delta_{d^2_x-y^2}(\boldsymbol{k}) \pm \sin\left(\frac{\pi}{3}\right)\Delta_{d_{xy}}(\boldsymbol{k})$ which minimalizes a free energy.

We apply the transformations

$$\begin{aligned} c_{\boldsymbol{k},\sigma} &= \frac{1}{\sqrt{2}}(a_{\boldsymbol{k},\sigma} - e^{i\cdot\phi_{\boldsymbol{k}}} b_{\boldsymbol{k},\sigma}), \\ d_{\boldsymbol{k},\sigma} &= \frac{1}{\sqrt{2}}(a_{\boldsymbol{k},\sigma} + e^{i\cdot\phi_{\boldsymbol{k}}} b_{\boldsymbol{k},\sigma}), \end{aligned} \tag{A.3}$$

such that in

see equation (A.4) above

diagonalize the kinetic part of the Hamiltonian. $C_{\boldsymbol{k}} = J\sum_{\boldsymbol{\delta}} \boldsymbol{\Delta}_{\boldsymbol{\delta}} \cos(\boldsymbol{k}\boldsymbol{\delta} - \phi_{\boldsymbol{k}})$ and $S_{\boldsymbol{k}} = J\sum_{\boldsymbol{\delta}} \boldsymbol{\Delta}_{\boldsymbol{\delta}} \sin(\boldsymbol{k}\boldsymbol{\delta} - \phi_{\boldsymbol{k}})$ are complex functions.

Here it is useful to split this Hamiltonian as $H_1 = H_1^{'} + H_1^{''}$ where

see equation (A.5) above

and

$$H_1^{''}(\boldsymbol{k}) = \begin{pmatrix} 0 & 0 & C_{\boldsymbol{k}} & 0 \\ 0 & 0 & 0 & -C_{\boldsymbol{k}} \\ C^*_{\boldsymbol{k}} & 0 & 0 & 0 \\ 0 & -C^*_{\boldsymbol{k}} & 0 & 0 \end{pmatrix}. \tag{A.7}$$

$H_1^{'}$ is diagonalized by

$$e_{\boldsymbol{k}+} = i\alpha^*_- c_{\boldsymbol{k}\uparrow} + \alpha_+ d^\dagger_{-\boldsymbol{k}\downarrow} \tag{A.8}$$

$$f_{\boldsymbol{k}+} = -i\alpha^*_- d_{\boldsymbol{k}\uparrow} + \alpha_+ c^\dagger_{-\boldsymbol{k}\downarrow} \tag{A.9}$$

with

$$\begin{aligned} \alpha_+ &= \sqrt{\frac{1}{2}\left(1 + \frac{\mu}{\sqrt{\mu^2 + |S_{\boldsymbol{k}}|^2}}\right)} \\ \alpha_- &= \frac{S_{\boldsymbol{k}}}{\sqrt{2\sqrt{\mu^2 + |S_{\boldsymbol{k}}|^2}\left(\mu + \sqrt{\mu^2 + |S_{\boldsymbol{k}}|^2}\right)}}. \end{aligned} \tag{A.10}$$

This leads to

$$H_2 = U_2 H_1 U_2^\dagger = \begin{pmatrix} e_1 & m & -l & 0 \\ m & e_2 & 0 & l \\ -l^* & 0 & -e_1 & m \\ 0 & l^* & m & -e_2 \end{pmatrix} \tag{A.11}$$

with

$$m = \frac{\mathrm{Re}(\mathrm{C}_{\boldsymbol{k}}) \cdot \mathrm{Im}(\mathrm{S}_{\boldsymbol{k}}) - \mathrm{Im}(\mathrm{C}_{\boldsymbol{k}}) \cdot \mathrm{Re}(\mathrm{S}_{\boldsymbol{k}})}{\sqrt{\mu^2 + |S_{\boldsymbol{k}}|^2}} \tag{A.12}$$

and

$$l = \alpha_+^2 C^*_{\boldsymbol{k}} + (\alpha^*_-)^2 C_{\boldsymbol{k}} \tag{A.13}$$

and $\pm e_1$ and $\pm e_2$ are eigenenergies of the Hamiltonian $H_1^{'}$ given by

$$e_1 = t|\gamma(\boldsymbol{k})| + \sqrt{\mu^2 + |S_{\boldsymbol{k}}|^2} \tag{A.14}$$

and

$$e_2 = -t|\gamma(\boldsymbol{k})| + \sqrt{\mu^2 + |S_{\boldsymbol{k}}|^2}. \tag{A.15}$$

We can now split this Hamiltonian as $H_2 = H_2^{'} + H_2^{''}$ where

$$H_2^{'} = \begin{pmatrix} e_1 & m & 0 & 0 \\ m & e_2 & 0 & 0 \\ 0 & 0 & -e_1 & m \\ 0 & 0 & m & -e_2 \end{pmatrix},$$
$$H_2^{''} = \begin{pmatrix} 0 & 0 & -l & 0 \\ 0 & 0 & 0 & l \\ -l^* & 0 & 0 & 0 \\ 0 & l^* & 0 & 0 \end{pmatrix}. \quad \text{(A.16)}$$

Proceeding now with the transformations

$$g_{\boldsymbol{k}+} = \beta_+ e_{\boldsymbol{k}+} + \sigma\beta_- f_{\boldsymbol{k}+} \quad \text{(A.17)}$$
$$h_{\boldsymbol{k}+} = \sigma\beta_- e_{\boldsymbol{k}+} - \beta_+ f_{\boldsymbol{k}+} \quad \text{(A.18)}$$

where $\sigma = \text{sign}(m)$ and

$$\beta_\pm = \sqrt{\frac{1}{2}\left(1 \pm \frac{t|\gamma(\boldsymbol{k})|}{\sqrt{t^2|\gamma(\boldsymbol{k})|^2 + m^2}}\right)} \quad \text{(A.19)}$$

we diagonalize first part of the Hamiltonian $H_2^{'}$ and we get

$$H_3 = U_3 H_2 U_3^\dagger = \begin{pmatrix} \epsilon_1 & 0 & 0 & -l \\ 0 & \epsilon_2 & -l & 0 \\ 0 & -l^* & -\epsilon_2 & 0 \\ -l^* & 0 & 0 & -\epsilon_1 \end{pmatrix} \quad \text{(A.20)}$$

where $\pm\epsilon_1$ and $\pm\epsilon_2$ are eigenenergies of the Hamiltonian $H_2^{'}$

$$\epsilon_1 = \sqrt{\mu^2 + |S_{\boldsymbol{k}}|^2} + \sqrt{t^2|\gamma(\boldsymbol{k})|^2 + m^2} \quad \text{(A.21)}$$

and

$$\epsilon_2 = \sqrt{\mu^2 + |S_{\boldsymbol{k}}|^2} - \sqrt{t^2|\gamma(\boldsymbol{k})|^2 + m^2}. \quad \text{(A.22)}$$

Finally, this Hamiltonian is brought to the diagonalized form with transformations

$$o_{\boldsymbol{k}+} = \gamma_+^{(1)} g_{\boldsymbol{k}+} - \gamma_-^{(1)} g_{\boldsymbol{k}-}^\dagger \quad \text{(A.23)}$$
$$p_{\boldsymbol{k}+} = \gamma_+^{(2)} h_{\boldsymbol{k}+} - \gamma_-^{(2)} h_{\boldsymbol{k}-}^\dagger \quad \text{(A.24)}$$

with

$$\gamma_+^{(1)} = \sqrt{\frac{1}{2}\left(1 + \frac{\epsilon_1}{E_\alpha}\right)},\ \gamma_-^{(1)} = \frac{l}{\sqrt{2E_\alpha\left(E_\alpha + \epsilon_1\right)}} \quad \text{(A.25)}$$

and

$$\gamma_+^{(2)} = \sqrt{\frac{1}{2}\left(1 + \frac{\epsilon_2}{E_\beta}\right)},\ \gamma_-^{(2)} = \frac{l}{\sqrt{2E_\beta\left(E_\beta + \epsilon_2\right)}} \quad \text{(A.26)}$$

and

$$E_\alpha = \sqrt{t^2|\gamma(\boldsymbol{k})|^2 + \mu^2 + |S_{\boldsymbol{k}}|^2 + |C_{\boldsymbol{k}}|^2 + 2\sqrt{u+v}} \quad \text{(A.27)}$$

and

$$E_\beta = \sqrt{t^2|\gamma(\boldsymbol{k})|^2 + \mu^2 + |S_{\boldsymbol{k}}|^2 + |C_{\boldsymbol{k}}|^2 - 2\sqrt{u+v}} \quad \text{(A.28)}$$

where

$$u = \left(\mu^2 + |S_{\boldsymbol{k}}|^2\right) t^2|\gamma(\boldsymbol{k})|^2$$
$$v = \left(\text{Re}C_{\boldsymbol{k}}\text{Im}S_{\boldsymbol{k}} - \text{Re}S_{\boldsymbol{k}}\text{Im}C_{\boldsymbol{k}}\right)^2. \quad \text{(A.29)}$$

Bogoliubov transformations $o_{\boldsymbol{k}+}$ and $p_{\boldsymbol{k}+}$ in the basis $a_{\boldsymbol{k}\uparrow}, b_{\boldsymbol{k},\uparrow}$

$$\begin{aligned} o_{\boldsymbol{k}+} = &-\frac{1}{\sqrt{2}}\left(\alpha_+\gamma_-^{(1)} - i\alpha_-^*\gamma_+^{(1)}\right)\left(\beta_+ - \sigma\beta_-\right) a_{\boldsymbol{k}\uparrow} \\ &- \frac{1}{\sqrt{2}} e^{i\phi_{\boldsymbol{k}}}\left(\alpha_+\gamma_-^{(1)} + i\alpha_-^*\gamma_+^{(1)}\right)\left(\beta_+ + \sigma\beta_-\right) b_{\boldsymbol{k}\uparrow} \\ &+ \frac{1}{\sqrt{2}}\left(\alpha_+\gamma_+^{(1)} + i\alpha_-\gamma_-^{(1)}\right)\left(\beta_+ + \sigma\beta_-\right) a_{-\boldsymbol{k}\downarrow}^\dagger \\ &+ \frac{1}{\sqrt{2}} e^{i\phi_{\boldsymbol{k}}}\left(\alpha_+\gamma_+^{(1)} - i\alpha_-\gamma_-^{(1)}\right)\left(\beta_+ - \sigma\beta_-\right) b_{-\boldsymbol{k}\downarrow}^\dagger \end{aligned} \quad \text{(A.30)}$$

$$\begin{aligned} p_{\boldsymbol{k}+} = &-\frac{1}{\sqrt{2}}\left(\alpha_+\gamma_-^{(2)} + i\alpha_-^*\gamma_+^{(2)}\right)\left(\beta_+ + \sigma\beta_-\right) a_{\boldsymbol{k}\uparrow} \\ &+ \frac{1}{\sqrt{2}} e^{i\phi_{\boldsymbol{k}}}\left(\alpha_+\gamma_-^{(2)} - i\alpha_-^*\gamma_+^{(2)}\right)\left(\beta_+ - \sigma\beta_-\right) b_{\boldsymbol{k}\uparrow} \\ &+ \frac{1}{\sqrt{2}}\left(\alpha_+\gamma_+^{(2)} - i\alpha_-\gamma_-^{(2)}\right)\left(\beta_+ - \sigma\beta_-\right) a_{-\boldsymbol{k}\downarrow}^\dagger \\ &- \frac{1}{\sqrt{2}} e^{i\phi_{\boldsymbol{k}}}\left(\alpha_+\gamma_+^{(2)} + i\alpha_-\gamma_-^{(2)}\right)\left(\beta_+ + \sigma\beta_-\right) a_{-\boldsymbol{k}\downarrow}^\dagger \end{aligned} \quad \text{(A.31)}$$

Appendix B: Correlation martix

B.1 s-wave scenario

The Hamiltonian equation (26) for s-wave superconductivity state in graphene can be diagonalized by using Bogoluibov transformations

$$\begin{aligned} e_{\boldsymbol{k}+} = &\alpha_+ \frac{1}{\sqrt{2}}(a_{\boldsymbol{k},\uparrow} - e^{i\cdot\phi_{\boldsymbol{k}}} b_{\boldsymbol{k},\uparrow}) \\ &+\alpha_- \frac{1}{\sqrt{2}}(a_{-\boldsymbol{k},\downarrow}^\dagger - e^{i\cdot\phi_{\boldsymbol{k}}} b_{-\boldsymbol{k},\downarrow}^\dagger) \end{aligned} \quad \text{(B.1)}$$

$$\begin{aligned} f_{\boldsymbol{k}+} = &\beta_- \frac{1}{\sqrt{2}}(a_{\boldsymbol{k},\uparrow} + e^{i\cdot\phi_{\boldsymbol{k}}} b_{\boldsymbol{k},\uparrow}) \\ &-\beta_+ \frac{1}{\sqrt{2}}(a_{-\boldsymbol{k},\downarrow}^\dagger + e^{i\cdot\phi_{\boldsymbol{k}}} b_{-\boldsymbol{k},\downarrow}^\dagger) \end{aligned} \quad \text{(B.2)}$$

where $\alpha_+ = \sqrt{\frac{1}{2}\left(1+\frac{t|\gamma(\boldsymbol{k})|-\mu}{\sqrt{(t|\gamma(\boldsymbol{k})|-\mu)^2+|C_{\boldsymbol{k}}|^2}}\right)}$, $\alpha_- = \frac{C_{\boldsymbol{k}}}{\sqrt{2E_\alpha(E_\alpha+t|\gamma(\boldsymbol{k})|-\mu)}}$, $\beta_+ = \sqrt{\frac{1}{2}\left(1+\frac{t|\gamma(\boldsymbol{k})|+\mu}{\sqrt{(t|\gamma(\boldsymbol{k})|+\mu)^2+|C_{\boldsymbol{k}}|^2}}\right)}$, and $\beta_- = \frac{C_{\boldsymbol{k}}}{\sqrt{2E_\beta(E_\beta+t|\gamma(\boldsymbol{k})|+\mu)}}$ with E_α and E_β are energies of Bogoliubov quasi-particles

$$E_\alpha = \sqrt{(t|\gamma(\boldsymbol{k})|-\mu)^2+|C_{\boldsymbol{k}}|^2} \tag{B.3}$$

and

$$E_\beta = \sqrt{(t|\gamma(\boldsymbol{k})|+\mu)^2+|C_{\boldsymbol{k}}|^2}. \tag{B.4}$$

The e (f) sections are determined by equations (B.1) and (B.2), respectively. These sections are decoupled in Bogoliubov description and we are allowed than to obtain their contributions to the ground state separative. We can demand $e_{\boldsymbol{k}+}|G\rangle = 0$ and $e^\dagger_{\boldsymbol{k}-}|G\rangle = 0$ where $|G\rangle$ is the ground state. The e section contributes to the ground state as:

$$\prod_{\boldsymbol{k}\in IBZ}\left(\alpha_+(\boldsymbol{k})-\alpha_-(\boldsymbol{k})c^\dagger_{\boldsymbol{k}\uparrow}c^\dagger_{-\boldsymbol{k}\downarrow}\right)|0\rangle \tag{B.5}$$

where $|0\rangle$ is the vacuum state. Similar, the contribution of the f section to the ground state:

$$\prod_{\boldsymbol{k}\in IBZ}\left(\beta_-(\boldsymbol{k})+\beta_+(\boldsymbol{k})d^\dagger_{\boldsymbol{k}\uparrow}d^\dagger_{-\boldsymbol{k}\downarrow}\right)|0\rangle \tag{B.6}$$

the ground state $|G\rangle$ is determined by conditions: $f_{\boldsymbol{k}+}|G\rangle = 0$ and $f^\dagger_{\boldsymbol{k}-}|G\rangle = 0$. This leads to the complete ground state vector:

$$\prod_{\boldsymbol{k}\in IBZ}\left(\alpha_+(\boldsymbol{k})-\alpha_-(\boldsymbol{k})c^\dagger_{\boldsymbol{k}\uparrow}c^\dagger_{-\boldsymbol{k}\downarrow}\right)\prod_{\boldsymbol{q}\in IBZ}\left(\beta_-(\boldsymbol{q})+\beta_+(\boldsymbol{q})d^\dagger_{\boldsymbol{q}\uparrow}d^\dagger_{-\boldsymbol{q}\downarrow}\right)|0\rangle. \tag{B.7}$$

Similar findings are obtained for the ground state of the p-wave superconductivity state in graphene [67].

This ground state leads to the correlation matrix when spin $\downarrow$ is traced out:

$$C(\boldsymbol{k}) = \begin{pmatrix} \frac{1}{2}\left(|\alpha_-|^2+|\beta_+|^2\right) & \frac{1}{2}e^{-i\phi_{\boldsymbol{k}}}\left(|\beta_+|^2-|\alpha_-|^2\right) \\ \frac{1}{2}e^{i\phi_{\boldsymbol{k}}}\left(|\beta_+|^2-|\alpha_-|^2\right) & \frac{1}{2}\left(|\alpha_-|^2+|\beta_+|^2\right)\end{pmatrix}. \tag{B.8}$$

B.2 Chiral d-wave scenario

Using

$$\begin{aligned} a_{\boldsymbol{k}\uparrow} = &-\frac{1}{\sqrt{2}}\left(\alpha_+\left(\gamma^{(1)}_-\right)^* + i\alpha_-\gamma^{(1)}_+\right)(\beta_+-\sigma\beta_-)\,o_{\boldsymbol{k},+} \\ &-\frac{1}{\sqrt{2}}\left(\alpha_+\left(\gamma^{(2)}_-\right)^* + i\alpha_-\gamma^{(2)}_+\right)(\beta_++\sigma\beta_-)\,p_{\boldsymbol{k},+} \\ &+\frac{1}{\sqrt{2}}\left(\alpha_+\gamma^{(2)}_+ - i\alpha_-\gamma^{(2)}_-\right)(\beta_++\sigma\beta_-)\,p^\dagger_{-\boldsymbol{k},-} \\ &+\frac{1}{\sqrt{2}}\left(\alpha_+\gamma^{(1)}_+ - i\alpha_-\gamma^{(1)}_-\right)(\beta_+-\sigma\beta_-)\,o^\dagger_{-\boldsymbol{k},-} \end{aligned} \tag{B.9}$$

we can calculate the mean occupancy at cite A:

$$\begin{aligned} \langle a^\dagger_{\boldsymbol{k}\uparrow}a_{\boldsymbol{k}\uparrow}\rangle = &\frac{1}{2}\Big(\alpha_+^2(\gamma^{(1)}_+)^2+|\alpha_-|^2|\gamma^{(1)}_-|^2 \\ &-i\,\alpha_+\gamma^{(1)}_+\left(\alpha_-\gamma^{(1)}_- - \alpha^*_-\left(\gamma^{(1)}_-\right)^*\right)\Big)(\beta_+-\sigma\beta_-)^2 \\ &+\frac{1}{2}\Big(\alpha_+^2(\gamma^{(2)}_+)^2+|\alpha_-|^2|\gamma^{(2)}_-|^2 - i\alpha_+\gamma^{(2)}_+\Big(\alpha_-\gamma^{(2)}_- \\ &-\alpha^*_-\left(\gamma^{(2)}_-\right)^*\Big)\Big)(\beta_++\sigma\beta_-)^2. \end{aligned} \tag{B.10}$$

After basic algebra we find that the correlation matrix obtained by tracing out spin $\downarrow$ at $T=0$ reads

$$C(\boldsymbol{k}) = \begin{pmatrix} C_{11}(\boldsymbol{k}) & C_{12}(\boldsymbol{k}) \\ C^*_{12}(\boldsymbol{k}) & C_{22}(\boldsymbol{k})\end{pmatrix} \tag{B.11}$$

with

$$\begin{aligned} C_{11}(\boldsymbol{k}) = &\frac{1}{2}\Big(\alpha_+^2(\gamma^{(1)}_+)^2+|\alpha_-|^2|\gamma^{(1)}_-|^2 - \alpha_+\gamma^{(1)}_+ \\ &\times\left(\alpha_-\gamma^{(1)}_- - \alpha^*_-\left(\gamma^{(1)}_-\right)^*\right)\Big)(\beta_+-\sigma\beta_-)^2 \\ &+\frac{1}{2}\Big(\alpha_+^2(\gamma^{(2)}_+)^2+|\alpha_-|^2|\gamma^{(2)}_-|^2 - i\alpha_+\gamma^{(2)}_+ \\ &\times\left(\alpha_-\gamma^{(2)}_- - \alpha^*_-\left(\gamma^{(2)}_-\right)^*\right)\Big)(\beta_++\sigma\beta_-)^2 \\ = &\frac{1}{2}+\frac{1}{4}\frac{\mu}{\sqrt{\mu^2+|S_{\boldsymbol{k}}|^2}}(\epsilon_1+m) \\ &\times\frac{1}{E_\alpha}\left(1-\frac{m}{\sqrt{t^2|\gamma(\boldsymbol{k})|^2+m^2}}\right) \\ &+\frac{1}{4}\frac{\mu}{\sqrt{\mu^2+|S_{\boldsymbol{k}}|^2}}(\epsilon_2+m) \\ &\times\frac{1}{E_\beta}\left(1+\frac{m}{\sqrt{t^2|\gamma(\boldsymbol{k})|^2+m^2}}\right), \end{aligned} \tag{B.12}$$

$$
\begin{aligned}
C_{22}(\boldsymbol{k}) = & \frac{1}{2}\left(\alpha_+^2(\gamma_+^{(1)})^2 + |\alpha_-|^2|\gamma_-^{(1)}|^2 + i\alpha_+\gamma_+^{(1)}\right. \\
& \left.\times\left(\alpha_-\gamma_-^{(1)} - \alpha_-^*\left(\gamma_-^{(1)}\right)^*\right)\right)(\beta_+ + \sigma\beta_-)^2 \\
& + \frac{1}{2}\left(\alpha_+^2(\gamma_+^{(2)})^2 + |\alpha_-|^2|\gamma_-^{(2)}|^2 + i\alpha_+\gamma_+^{(2)}\right. \\
& \left.\times\left(\alpha_-\gamma_-^{(2)} - \alpha_-^*\left(\gamma_-^{(2)}\right)^*\right)\right)(\beta_+ - \sigma\beta_-)^2 \\
= & \frac{1}{2} + \frac{1}{4}\frac{\mu}{\sqrt{\mu^2 + |S_{\boldsymbol{k}}|^2}}(\epsilon_1 - m) \\
& \times \frac{1}{E_\alpha}\left(1 + \frac{m}{\sqrt{t^2|\gamma(\boldsymbol{k})|^2 + m^2}}\right) \\
& + \frac{1}{4}\frac{\mu}{\sqrt{\mu^2 + |S_{\boldsymbol{k}}|^2}}(\epsilon_2 - m) \\
& \times \frac{1}{E_\beta}\left(1 - \frac{m}{\sqrt{t^2|\gamma(\boldsymbol{k})|^2 + m^2}}\right), \qquad \text{(B.13)}
\end{aligned}
$$

and

$$
\begin{aligned}
C_{12}(\boldsymbol{k}) = & \frac{1}{2}e^{-i\phi_{\boldsymbol{k}}}\left(\alpha_+^2(\gamma_+^{(1)})^2 - |\alpha_-|^2|\gamma_-^{(1)}|^2 - i\alpha_+\gamma_+^{(1)}\right. \\
& \left.\times\left(\alpha_-^{(1)}\gamma_-^{(1)} + \left(\alpha_-^{(1)}\right)^*\left(\gamma_-^{(1)}\right)^*\right)\right)(\beta_+^2 - \beta_-^2) \\
& - \frac{1}{2}e^{-i\phi_{\boldsymbol{k}}}\left(\alpha_+^2(\gamma_+^{(2)})^2 - |\alpha_-|^2|\gamma_+^{(2)}|^2 - i\alpha_+\gamma_+^{(2)}\right. \\
& \left.\times\left(\alpha_-^{(1)}\gamma_-^{(2)} + \left(\alpha_-^{(1)}\right)^*\left(\gamma_-^{(2)}\right)^*\right)\right)(\beta_+^2 - \beta_-^2) \\
= & \frac{1}{4}e^{-i\phi_{\boldsymbol{k}}}\left(\left(\frac{\epsilon_1}{E_\alpha} - \frac{\epsilon_2}{E_\beta}\right)\right. \\
& \left. - i\,n\left(\frac{1}{E_\alpha} - \frac{1}{E_\beta}\right)\right)\frac{t|\gamma(\boldsymbol{k})|}{\sqrt{t^2|\gamma(\boldsymbol{k})|^2 + m^2}} \qquad \text{(B.14)}
\end{aligned}
$$

where $n = \frac{\mathrm{Re}(C_{\boldsymbol{k}})\mathrm{Re}(S_{\boldsymbol{k}}) + \mathrm{Im}(C_{\boldsymbol{k}})\mathrm{Im}(S_{\boldsymbol{k}})}{\sqrt{\mu^2 + |S_{\boldsymbol{k}}|^2}}$. Here, one should notice that $C_{11}(-\boldsymbol{k}) = C_{22}(\boldsymbol{k})$ and $C_{12}(\boldsymbol{k}) = (C_{12}(-\boldsymbol{k}))^*$.

Eigenvectors of the correlation matrix

$$
q_{\boldsymbol{k}\uparrow} = \delta_+(\boldsymbol{k})a_{\boldsymbol{k}\uparrow} + \delta_-(\boldsymbol{k})b_{\boldsymbol{k}\uparrow} \qquad \text{(B.15)}
$$

$$
r_{\boldsymbol{k}\uparrow} = \delta_+(-\boldsymbol{k})a_{\boldsymbol{k}\uparrow} - \delta_-^*(-\boldsymbol{k})b_{\boldsymbol{k}\uparrow} \qquad \text{(B.16)}
$$

where:

$$
\begin{aligned}
\delta_+(\boldsymbol{k}) &= \sqrt{\frac{1}{2}\left(1 + \frac{C_{11} - C_{22}}{\sqrt{(C_{11} - C_{22})^2 + 4|C_{12}|^2}}\right)} \\
\delta_-(\boldsymbol{k}) &= \frac{2C_{12}}{\sqrt{2\sqrt{(C_{11} - C_{22})^2 + 4|C_{12}|^2}w}} \qquad \text{(B.17)}
\end{aligned}
$$

with $w = (C_{11} - C_{22} + \sqrt{(C_{11} - C_{22})^2 + 4|C_{12}|^2})$.

Finally, we find that the correlation matrix obtained by tracing out one sublattice, B for example

$$
C(\boldsymbol{k}) = \begin{pmatrix} C_{11}(\boldsymbol{k}) & C_{13}(\boldsymbol{k}) \\ C_{13}^*(\boldsymbol{k}) & C_{33}(\boldsymbol{k}) \end{pmatrix} \qquad \text{(B.18)}
$$

with

$$
\begin{aligned}
C_{11}(\boldsymbol{k}) = & \frac{1}{2}\left(\alpha_+^2(\gamma_+^{(1)})^2 + |\alpha_-|^2|\gamma_-^{(1)}|^2 - i\alpha_+\gamma_+^{(1)}\right. \\
& \left.\times\left(\alpha_-\gamma_-^{(1)} - \alpha_-^*\left(\gamma_-^{(1)}\right)^*\right)\right)(\beta_+ - \sigma\beta_-)^2 \\
& + \frac{1}{2}\left(\alpha_+^2(\gamma_+^{(2)})^2 + |\alpha_-|^2|\gamma_-^{(2)}|^2 - i\alpha_+\gamma_+^{(2)}\right. \\
& \left.\times\left(\alpha_-\gamma_-^{(2)} - \alpha_-^*\left(\gamma_-^{(2)}\right)^*\right)\right)(\beta_+ + \sigma\beta_-)^2 \\
= & \frac{1}{2} + \frac{1}{4}\frac{\mu}{\sqrt{\mu^2 + |S_{\boldsymbol{k}}|^2}}(\epsilon_1 + m) \\
& \times \frac{1}{E_\alpha}\left(1 - \frac{m}{\sqrt{t^2|\gamma(\boldsymbol{k})|^2 + m^2}}\right) \\
& + \frac{1}{4}\frac{\mu}{\sqrt{\mu^2 + |S_{\boldsymbol{k}}|^2}}(\epsilon_2 + m) \\
& \times \frac{1}{E_\beta}\left(1 + \frac{m}{\sqrt{t^2|\gamma(\boldsymbol{k})|^2 + m^2}}\right), \qquad \text{(B.19)}
\end{aligned}
$$

$$
\begin{aligned}
C_{33}(\boldsymbol{k}) = & \frac{1}{2}\left(\alpha_+^2(\gamma_-^{(1)})^2 + |\alpha_-|^2|\gamma_+^{(1)}|^2 - i\alpha_+\gamma_+^{(1)}\right. \\
& \left.\times\left(\alpha_-\gamma_-^{(1)} - \alpha_-^*\left(\gamma_-^{(1)}\right)^*\right)\right)(\beta_+ + \sigma\beta_-)^2 \\
& + \frac{1}{2}\left(\alpha_+^2(\gamma_-^{(2)})^2 + |\alpha_-|^2|\gamma_+^{(2)}|^2 - i\alpha_+\gamma_+^{(2)}\right. \\
& \left.\times\left(\alpha_-\gamma_-^{(2)} - \alpha_-^*\left(\gamma_-^{(2)}\right)^*\right)\right)(\beta_+ - \sigma\beta_-)^2 \\
= & \frac{1}{2} - \frac{1}{4}\frac{\mu}{\sqrt{\mu^2 + |S_{\boldsymbol{k}}|^2}}(\epsilon_1 - m) \\
& \times \frac{1}{E_\alpha}\left(1 + \frac{m}{\sqrt{t^2|\gamma(\boldsymbol{k})|^2 + m^2}}\right) \\
& - \frac{1}{4}\frac{\mu}{\sqrt{\mu^2 + |S_{\boldsymbol{k}}|^2}}(\epsilon_2 - m) \\
& \times \frac{1}{E_\beta}\left(1 - \frac{m}{\sqrt{t^2|\gamma(\boldsymbol{k})|^2 + m^2}}\right), \qquad \text{(B.20)}
\end{aligned}
$$

and

$$
\begin{aligned}
C_{13}(\boldsymbol{k}) = & \frac{1}{2}\left(\alpha_+^2\left(\gamma_+^{(1)}\gamma_-^{(1)} - \gamma_+^{(2)}\gamma_-^{(2)}\right) - \left(\alpha_-^*\right)^2\left(\gamma_+^{(1)}\right.\right. \\
& \left.\left.\times(\gamma_-^{(1)})^* - \gamma_+^{(2)}(\gamma_-^{(2)})^*\right)\right)(\beta_+^2 - \beta_-^2) \\
= & \frac{1}{4}\left(\frac{1}{E_\alpha} - \frac{1}{E_\beta}\right)\frac{\mu}{\sqrt{\mu^2 + |S_{\boldsymbol{k}}|^2}} \\
& \times \frac{t|\gamma(\boldsymbol{k})|}{\sqrt{t^2|\gamma(\boldsymbol{k})|^2 + m^2}}C_{\boldsymbol{k}}^*. \qquad \text{(B.21)}
\end{aligned}
$$

References

1. B. Uchoa, A.H. Castro Neto, Phys. Rev. Lett. **98**, 146801 (2007)
2. A.M. Black-Schaffer, S. Doniach, Phys. Rev. B **75**, 134512 (2007)
3. C. Honerkamp, Phys. Rev. Lett. **100**, 146404 (2008)
4. S. Pathak, V.B. Shenoy, G. Baskaran, Phys. Rev. B **81**, 085431 (2010)
5. R. Nandkishore, L.S. Levitov, A.V. Chubukov, Nat. Phys. **8**, 158 (2011)
6. M. Kiesel, C. Platt, W. Hanke, D.A. Abanin, R. Thomale, Phys. Rev. B **86**, 020507(R) (2012)
7. W. S. Wang, Y.Y. Xiang, Q.-H. Wang, F. Wang, F. Yang, D.-H. Lee, Phys. Rev. B **85**, 035414 (2012)
8. M.V. Milovanović, S. Predin, Phys. Rev. B **86**, 195113 (2012)
9. J. Vučičević, M.O. Goerbig, M.V. Milovanović, Phys. Rev. B **86**, 214505 (2012)
10. O. Vafek, J.M. Murray, V. Cvetkovic, Phys. Rev. Lett. **112**, 147002 (2014)
11. A.M. Black-Schaffer, C. Honerkamp, J. Phys.: Condens. Matter **26**, 423201 (2014)
12. C. Platt, W. Hanke, R. Thomale, Adv. Phys. **62**, 453 (2013)
13. S. Ichinokura, K. Sugawara, A. Takayama, T. Takahashi, S. Hasegawa, ACS Nano **10**, 2761 (2016)
14. J. Chapman, Y. Su, C.A. Howard, D. Kundys, A.N. Grigorenko, F. Guinea, A.K. Geim, I.V. Grigorieva, R.R. Nair, Sci. Rep. **6**, 23254 (2016)
15. B.M. Ludbrook, G. Levy, P. Nigge, M. Zonno, M. Schneider, D.J. Dvorak, C.N. Veenstra, S. Zhdanovich, D. Wong, P. Dosanjh, C. Straßer, A. Stöhr, S. Forti, C.R. Ast, U. Starke, A. Damascelli, Proc. Natl. Acad. Sci. **112**, 11795 (2015)
16. M. Levin, X.-G. Wen, Phys. Rev. Lett. **96**, 110405 (2006)
17. A. Kitaev, J. Preskill, Phys. Rev. Lett. **96**, 110404 (2006)
18. H.-C. Jiang, Z. Wang, L. Balents, Nat. Phys. **8**, 902 (2012)
19. H. Li, F.D.M. Haldane, Phys. Rev. Lett. **101**, 010504 (2008)
20. N. Bray-Ali, L. Ding, S. Haas, Phys. Rev. B **80**, 180504 (2009)
21. A.M. Läuchli, E.J. Bergholtz, J. Suorsa, M. Haque, Phys. Rev. Lett. **104**, 156404 (2010)
22. H. Yao, X.-L. Qi, Phys. Rev. Lett. **105**, 080501 (2010)
23. E. Prodan, T.L. Hughes, B.A. Bernevig, Phys. Rev. Lett. **105**, 115501 (2010)
24. R. Thomale, A. Sterdyniak, N. Regnault, B.A. Bernevig, Phys. Rev. Lett. **104**, 180502 (2010)
25. A.M. Turner, Y. Zhang, A. Vishwanath, Phys. Rev. B **82**, 241102 (2010)
26. L. Fidkowski, Phys. Rev. Lett. **104**, 130502 (2010)
27. F. Pollmann, A.M. Turner, E. Berg, M. Oshikawa, Phys. Rev. B **81**, 064439 (2010)
28. M. Kargarian, G.A. Fiete, Phys. Rev. B **82**, 085106 (2010)
29. M. Hermanns, A. Chandran, N. Regnault, B.A. Bernevig, Phys. Rev. B **84**, 121309 (2011)
30. J. Dubail, N. Read, Phys. Rev. Lett. **107**, 157001 (2011)
31. N. Regnault, B.A. Bernevig, Phys. Rev. X **1**, 021014 (2011)
32. Z. Papić, B.A. Bernevig, N. Regnault, Phys. Rev. Lett. **106**, 056801 (2011)
33. T.L. Hughes, E. Prodan, B.A. Bernevig, Phys. Rev. B **83**, 245132 (2011)
34. X.-L. Qi, H. Katsura, A.W.W. Ludwig, Phys. Rev. Lett. **108**, 196402 (2012)
35. D. Poilblanc, N. Schuch, D. Perez-Garcia, J.I. Cirac, Phys. Rev. B **86**, 014404 (2012)
36. B. Swingle, T. Senthil, Phys. Rev. B **86**, 045117 (2012)
37. N. Regnault, arXiv:1510.07670 (2015)
38. N. Laflorencie, Phys. Rep. **643**, 1 (2016)
39. A. Chandran, V. Khemani, S.L. Sondhi, Phys. Rev. Lett. **113**, 060501 (2014)
40. H. Braganca, E. Mascarenhas, G.I. Luiz, C. Duarte, R.G. Pereira, M.F. Santos, M.C.O. Aguiar, Phys. Rev. B **89**, 235132 (2014)
41. R. Lundgren, J. Blair, M. Greiter, A. Läuchli, G.A. Fiete, R. Thomale, Phys. Rev. Lett. **113**, 256404 (2014)
42. D. Poilblanc, Phys. Rev. Lett. **105**, 077202 (2010)
43. J.I. Cirac, D. Poilblanc, N. Schuch, F. Verstraete, Phys. Rev. B **83**, 245134 (2011)
44. I. Peschel, M.-C. Chung, Europhys. Lett. **96**, 50006 (2011)
45. A.M. Läuchli, J. Schliemann, Phys. Rev. B **85**, 054403 (2012)
46. J. Schliemann, A.M. Läuchli, J. Stat. Mech. **2012**, P11021 (2012)
47. S. Tanaka, R. Tamura, H. Katsura, Phys. Rev. A **86**, 032326 (2012)
48. R. Lundgren, Y. Fuji, S. Furukawa, M. Oshikawa, Phys. Rev. B **88**, 245137 (2013)
49. X. Chen, E. Fradkin, J. Stat. Mech. **2013**, P08013 (2013)
50. R. Lundgren, Phys. Rev. B **93**, 125107 (2016)
51. J. Schliemann, Phys. Rev. B **83**, 115322 (2011)
52. J. Schliemann, New J. Phys. **15** 053017 (2013), Corrigendum: **15**, 079501 (2013)
53. J. Schliemann, J. Stat. Mech. **2014**, P09011 (2014)
54. R. Lundgren, V. Chua, G.A. Fiete, Phys. Rev. B **86**, 224422 (2012)
55. S. Predin, P. Wenk, J. Schliemann, Phys. Rev. B **93**, 115106 (2016)
56. T. Fukui, Y. Hatsugai, J. Phys. Soc. Jpn. **83**, 113705 (2014)
57. H. Araki, T. Kariyado, T. Fukui, Y. Hatsugai, arXiv:1602.02910 (2016)
58. D. Poletti, C. Miniatura, B. Gremaud, Europhys. Lett. **93**, 37008 (2011)
59. M. Sato, S. Fujimoto, J. Phys. Soc. Jpn. **85**, 072001 (2016)
60. A. Altland, M.R. Zirnbauer, Phys. Rev. B, **55**, 1142 (1997)
61. A.P. Schnyder, S. Ryu, A. Furusaki, A.W.W. Ludwig, Phys. Rev. B **78**, 195125 (2008)
62. I. Peschel, J. Phys. A: Math. Gen. **36**, L205 (2003)
63. S.-A. Cheong, C.L. Henley, Phys. Rev. B **69**, 075111 (2004)
64. J. Borchmann, A. Farrell, S. Matsuura, T. Pereg-Barnea, Phys. Rev. B **90**, 235150 (2014)
65. E.H. Kim, J. Phys.: Condens. Matter **26**, 205602 (2014)
66. A.M. Black-Schaffer, K. Le Hur, Phys. Rev. B **92**, 140503(R) (2015)
67. M.V. Milovanović, arXiv:1102.2576 (2011)